UNIVERSITY OF CALIFORNIA

Los Angeles

Suturable Elastin-based Fibrous Patch for Urinary Tract Reconstruction

A thesis submitted in partial satisfaction of the

requirements for the degree Master of Science

in Chemical Engineering

by

Yadi Huo

2023

ABSTRACT OF THE THESIS

Suturable Elastin-based Fibrous Patch for Urinary Tract Reconstruction

by

Yadi Huo

Master of Science in Chemical Engineering

University of California, Los Angeles, 2023

Professor Nasim Annabi, Chair

The application of engineered biomimetic materials in surgical reconstruction presents a promising avenue for repairing damaged urinary tract tissues. Current autografts from skin and buccal mucosa are limited due to lack of tissue availability, donor site morbidity, and inadequate elasticity. Hydrogel-based biomaterials with high water content and permeability show promise in mimicking the native tissue environment. Despite their potential, the clinical application of hydrogels has been constrained by factors such as inadequate mechanical properties, and unpredictable degradation rates. Here, we present the development of a photocrosslinked suturable elastic fibrous hydrogel comprised of gelatin methacryloyl (GelMA) and an elastin-like polypeptide (ELP) using an electrospinning technology designed to repair or replace urologic tissues. The fabrication of hybrid hydrogels with tailored physical properties, achieved by modulating GelMA and ELP concentrations, enabled an appropriate match for urological tissue reconstruction, as established through comparisons with native rabbit urethral and bladder tissues.

In addition, the abilities of the engineered scaffolds to physically support tissue repair were further confirmed through suture retention and *ex vivo* bladder repair tests. These evaluations demonstrated an enhanced capacity of the scaffolds to sustain integrity and promote tissue defect repair, suggesting their potential therapeutic relevance in the field of urological tissue regeneration. Moreover, enzymatic degradation profiles demonstrated that the GelMA/ELP scaffolds can be degraded while preserving the structures over a sufficient period to facilitate tissue regeneration. Furthermore, the composite fibrous hydrogels showed remarkable biocompatibility and supported cell growth, spreading, and proliferation of human cell lines.

The thesis of Yadi Huo is approved.

Thaiesha Andrea Wright

Renea Michelle Sturm

Nasim Annabi, Committee Chair

University of California, Los Angeles

2023

Table of Contents

LIST OF FIGURES

Actin (red)/DAPI (blue) stained images from urothelial cells seeded on (f) 0E10G and (g) at day 1 and representative Actin (red)/DAPI (blue) stained images from urothelial cells seeded on (h) 0E10G and (i) at day 7 post culture. Quantification (j) metabolic activity of urothelial cells seeded on scaffolds after 1, 3, 5 and 7 days of culture. (* $p < 0.05$, ** $p < 0.01$, *** $p < 0.001$).

Figure S1. Mechanical properties of male rabbits urologic tissues, GelMA/ELP fibrous scaffolds, and the degradation profiles of additional compositions of GelMA/ELP scaffolds. (a) Ultimate strength, (b) Extensibility, and (c) Tensile Young's modulus of regular and decellularized rabbit urinary tract tissues. (d) Representative tensile stress–strain curves of different composite GelMA/ELP scaffolds and urinary tract tissues. Representative tensile cyclic loading and unloading curves of 10 cycles for (e) 5E5G scaffolds and for (f) rabbit urethra tissues. (g) 3E7G, and (h) 7E3G degradation profiles with and without the presence of collagenase and elastase. (* $p < 0.05$, ** $p < 0.01$, *** $p < 0.001$, **** $p < 0.0001$).

Figure S2. *In vitro* cytocompatibility of GelMA/ELP fibrous scaffolds using fibroblast cells. Representative live/dead images from fibroblast cells seeded on (a) 0E10G and (b) 5E5G scaffolds at day 1, and representative live/dead images from fibroblast cells of seeding on (c) 0E10G and (d) 5E5G scaffolds. Quantification of (e) viability after 1, 5 and 7 days of culture. Representative Actin (red)/DAPI (blue) stained images from fibroblast cells seeded on (f) 0E10G and (g) at day 1 and representative Actin (red)/DAPI (blue) stained images from fibroblast cells seeded on (h) 0E10G and (i) at day 7 post culture. Quantification (j) metabolic activity of urothelial cells seeded on scaffolds after 1, 3, 5 and 7 days of culture. (* $p < 0.05$, ** $p < 0.01$, *** $p < 0.001$).

ACKNOWLEDGEMENT

First and foremost, I want to express my deepest gratitude to Dr. Nasim Annabi for her unwavering guidance, steadfast mentorship, and consistent support throughout this challenging, yet rewarding, journey.

I would also like to extend my sincere appreciation to Dr. Sturm. Her insightful advice and constructive suggestions have been invaluable to the evolution and refinement of my work.

Special thanks are in order for my colleagues - Felix, Ronak, and Yavuz. Their collaborations have significantly enriched my work. Their support, both professionally and personally, has been instrumental in the successful completion of this thesis.

Furthermore, I am extremely grateful for the camaraderie and support from Yuting, Annabella, Yimin, and Albert. Their friendship has transformed our lab into a second home, making the arduous process of conducting research both enjoyable and rewarding.

Above all, my heartfelt thanks go to my parents, Huiqin Yang and Xiaorong Huo. Their unwavering trust, endless support, and immeasurable love have been my strongest pillars. They have not just been my parents but also my most cherished cheerleaders, supporting me in every step of this journey.

Thanks most of all to Lingjie for his patience, understanding, and inspiration. His constant presence by my side, as my best friend and most loyal supporter, has always given me immense strength and confidence.

INTRODUCTION

Biomimetic reconstruction strategies for various living tissues are a growing field in tissue engineering.[1-4] The utilization of scaffolds with biomimetic characteristics has shown great potential for promoting the reconstruction of damaged tissues and restoring their functionality. However, there are still significant challenges to overcome in the regenerative engineering of intricate tissue-based architectures. The urethra not only plays a crucial role in the urinary system for transporting urine from the bladder to the external environment but also functions as a conduit for semen during ejaculation in males.[5] The integrity and proper functioning of urethral tissue are essential for the normal flow and control of urine, as well as for reproductive processes. Urethral tissue damage or abnormalities can arise most commonly from hypospadias (a common congenital deformity) or urethral stricture (narrowing of the urethral lumen). Symptoms of these conditions can include urinary obstruction, urinary tract infections, pain, and discomfort.[6-8]

The male urethra in its natural form is composed of three distinct primary cell types, existing in a layered fashion: the urethral epithelium, fibroblasts, and smooth muscle cells (SMC).[9, 10] The urethral epithelium, which lines the inner surface, undergoes changes in its characteristics along the length of the urethra. Currently, autologous grafts or flaps from genital skin and buccal mucosa are commonly used for urethral reconstruction.[11, 12] However, autologous grafts can be limited by inadequate tissue and can result in donor site morbidity,[11] such as contracture or effects on salivation or sensation. Additionally, these tissues fail to recapitulate the unique elastic properties of the urethral lumen, which undergoes considerable mechanical stress and must be capable of frequent radial expansion and contraction according to the natural excretion of urine from the body as well as longitudinal extensibility during penile erection. The use of skin grafts in genitourinary reconstructive surgery can lead to potential infections due to hair growth and the formation of

stones in the reconstructed urethra.[13] Additionally, there are limitations in utilizing depilated skin from patients with lichen sclerosis. Research has shown that fibroblasts in lichen sclerosis-affected skin have increased collagen secretion activity compared to healthy skin. This heightened activity can contribute to the narrowing of the urethra, further complicating the condition. Furthermore, the size of tissue graft that can be obtained from a donor site is limited, particularly when dealing with long urethral defects.

Based on the physiological and anatomical characteristics of the urethra, an ideal tissue-engineered graft should aim to replicate the structural and functional properties of the native urethral tissue. This includes good biocompatibility to promote cell adhesion, and highly permeable and 3D fiber structure to mimic the extracellular matrix (ECM) to facilitate cell migration and cell-cell adhesion to ensure a protective barrier against urine. The engineered graft should also have a high-water content and promote vascularization to ensure cell metabolism and proper blood supply. Furthermore, it should also be able to withstand mechanical forces during surgical procedures. By attempting these objectives, a tissue-engineered graft can closely resemble the native urethra both in structure and function.

Hydrogels are three-dimensional (3D) polymeric materials with high water content and high permeability for the diffusion of essential nutrients and oxygen, which support cell migration and cell metabolism.[14, 15] Hydrogels have been extensively used in various areas of regenerative medicine and tissue engineering due to their potential abilities to mimic the properties of ECM environment present in native tissues.[16, 17] In order to modulate the physiological response in cells and tissues, and to mimic the mechanical, biochemical, and topographical properties of urological tissues, both natural and synthetic polymers, along with a range of fabrication techniques have been reported to design and manufacture hydrogels with appropriate physicochemical properties.

[18, 19] These polymers, either individually or in combination with other polymers, can be employed to fabricate composite hydrogels that possess improved properties suitable for their application as urethral grafts. Here, we review the major biomaterials that have been reported for their potential in urethral reconstruction applications by comparing their resulting mechanical and physiological properties. Furthermore, we review the current advanced fabrication techniques utilized in urethral tissue engineering. These techniques include electrospinning, 3D printing, and molding.

1. Critical Literature Review

In this section, we first review different biomaterials that have been used for urinary tract reconstructions. These natural and synthetic biomaterials possess distinct advantages and limitations that influence their applications (Table 1). Subsequently, we summarized the method of electrospinning and recent studies that utilize this technique to construct grafts intended for urological applications (Table 2).

1.1. Natural and synthetic biomaterials used for urologic tissue reconstruction

1.1.1 Protein-based biomaterials

In the realm of urological tissue engineering, collagen has been explored for its potential to reconstruct various urologic tissues, given its ability to simulate the natural ECM environment, which plays a crucial role in maintaining structural integrity and directing cell behavior.[18] It can also provide cells with a natural environment, facilitating proliferation, migration, and differentiation. For instance, Zhang *et al*. successfully used collagen scaffolds for the repair of urethral defects in a rabbit model, demonstrating significant regeneration of urethral tissue with well-organized smooth muscle layers.[20] Additionally, collagen has been incorporated into hybrid scaffolds with synthetic polymers to improve mechanical properties and biocompatibility, as seen in the work by Fu *et al*. for bladder augmentation.[21] Despite these advancements, challenges

remain, particularly regarding the mechanical strength of collagen-based scaffolds and their rate of degradation *in vivo*. These are crucial factors that must be considered when designing collagen-based scaffolds for urological tissue engineering applications.

Silk fibroin (SF), a natural protein polymer derived primarily from silkworms, boasts unique properties such as excellent mechanical strength, flexibility, and biocompatibility.[22] It is also characterized by its superior processability, enabling the formation of various structures, such as films, hydrogels, and fibrous matrices, making it a material of interest in the realm of tissue engineering. Within urological tissue engineering, SF has been explored for its potential in various applications, owing to its tunable degradation rate and ability to support cell attachment, proliferation, and differentiation. For instance, in research conducted by Namata *et al*., a novel approach was taken wherein SF-based scaffolds were used to engineer patient-specific implants for bladder augmentation, demonstrating a promising strategy for future clinical applications.[23] Furthermore, Kim *et al*. demonstrated that electrospun SF scaffolds could promote the proliferation and matrix deposition of fibroblasts, a key cell type involved in urethral tissue regeneration.[24] These examples underline the promising role of silk fibroin in the reconstruction of urological tissues. Nevertheless, some challenges need to be addressed, such as the inconsistent degradation rate of SF *in vivo* and potential immune responses. Such considerations are critical in the design and application of SF-based scaffolds for urological tissue engineering applications.

Elastin-like polypeptides (ELPs) are biopolymers produced from recombinant Escherichia coli (*E. coli*) resembling native elastin. ELPs have gained significant interest in the field of tissue engineering due to their unique physicochemical properties and potential for genetic design. These polymers are not only biocompatible and biodegradable but also exhibit excellent elasticity, which

is one of the key factors to consider in urinary tract tissue engineering.[25] Despite its potential for urinary tract reconstruction, specific research on this topic is not yet available.

1.1.2 Polysaccharide-based biomaterials

Hyaluronic acid (HA), a natural glycosaminoglycan, is an integral component of the ECM that plays critical roles in cell proliferation, migration, and differentiation due to its significant hydration and viscoelastic properties.[26] Because of its excellent biocompatibility and hygroscopic properties, HA has been extensively employed as a biomaterial in a range of tissue engineering applications, including urological tissue reconstruction due to its innate ability to mimic the natural ECM environment. For example, in a study by Bury *et al*., HA was incorporated into a collagen scaffold for bladder augmentation, leading to improved cell proliferation and bladder function.[27] Another notable application of HA was demonstrated by Özok *et al*., who used a dextranomer/HA copolymer as a bladder neck injection for treating urinary incontinence, indicating its potential in restoring urinary function.[28] Despite these advancements, challenges remain with HA-based scaffolds, particularly concerning their mechanical properties and *in vivo* degradation rates. These are critical considerations when designing HA-based scaffolds for urological tissue engineering applications.

Alginate, a naturally occurring polysaccharide derived from brown algae, has been widely used in the field of tissue engineering due to its excellent biocompatibility, low cost, and gelation properties.[29] In the domain of urological tissue engineering, alginate has shown great potential due to its ability to form a scaffold for bladder reconstruction, while also showing promise in promoting cell adhesion, proliferation, and differentiation. For example, Kurowiak *et al*. developed an alginate-based hydrogel with the addition of African plum bark and showed its potential use in urethral reconstruction due to its excellent elasticity.[30] Nonetheless, challenges

with alginate, such as its relatively weak mechanical properties and rapid degradation, continue to be areas of ongoing research to optimize its use in urological applications.

Chitosan (CS), a naturally derived polysaccharide derived from the exoskeletons of crustaceans, exhibits many attractive characteristics for tissue engineering. It is biocompatible, biodegradable, has antimicrobial properties, and can promote wound healing and cell proliferation.[31] CS scaffolds, for instance, have been employed in the repair of bladder defects. In one such study by Hajiabbas *et al*., chitosan-gelatin scaffolds were seeded with bladder smooth muscle cells and demonstrated good cell adhesion and proliferation, supporting the potential of CS for bladder tissue engineering.[32] Notwithstanding these advancements, challenges persist in optimizing the mechanical properties and degradation rate of chitosan-based scaffolds for urological tissue engineering, making it a critical area for ongoing research.

1.1.3 Decellularized tissue-derived biomaterials

Small intestine submucosa (SIS), a decellularized natural biomaterial derived from the submucosa of porcine small intestine, has been recognized for its potential in tissue engineering owing to its superior biocompatibility, biodegradability, and ability to promote cell proliferation and differentiation.[32] Wu *et al*. successfully used modified 3D SIS scaffolds seeded with human urine-derived stem cells to promote urethral tissue regeneration, showing that SIS can serve as an effective biomaterial for urethral repair.[33] Palminteri *et al*. have shown the considerable potential of using SIS in urological applications. In their study, the researchers achieved a 94% success rate in short-term bulbar urethroplasty by employing SIS as an acellular urethroplasty matrix.[34] This showed SIS ability to support tissue regeneration and to function as an effective matrix for urethroplasty. Further, a medium-term follow-up study conducted by Fiala *et al*. reported an 80% success rate after an average of 31 months, following the use of SIS grafts, primarily for penile

stricture repair.[35] This result not only affirms the potential of SIS in urological tissue engineering but also demonstrates its durability and long-term effectiveness. In contrast, a study conducted by Raber *et al*. demonstrated less favorable results with the use of acellular SIS grafts for urethroplasty.[36] Among the five patients in the study, four required re-intervention due to stricture recurrence within an average period of 12 months. This suggests that while SIS may demonstrate promise as a biomaterial for urological tissue engineering, the potential for complications, such as stricture recurrence, cannot be overlooked. This research is a reminder that the optimal biomaterial for urethroplasty might still need to be determined, and extended clinical trials are needed to ensure that the materials developed enhance the outcomes of these procedures.

1.1.4 Synthetic biomaterials

While hydrogels derived from biopolymers can mimic the architecture and mechanical properties of the ECM, they present challenges in customization and manipulation. Conversely, synthetic fibrous gels, when combined with on-demand adaptivity, offer the potential for highly tailorable materials. Thus, an ideal approach may involve integrating the intrinsic biological benefits of biopolymers with the versatility and adaptability of synthetic polymers, producing an optimal scaffold for tissue engineering applications.[37]

Synthetic polymers, notably poly(lactic acid) (PLA), poly(lactic-co-glycolic acid) (PLGA), and poly(glycolic acid) (PGA), are among the most widely utilized materials in tissue regeneration. In a study by Pattison *et al*., PLGA 3D porous scaffolds have shown promising *in vivo* replacements for the urinary bladder wall.[38] The authors reported improved bladder capacity and compliance, with histological analysis revealing formation of multiple layers of urothelial cells. Kanematsu *et al*. utilized PLGA scaffolds for bladder augmentation in a rat model.[39] The PLGA scaffolds showed successful regeneration of bladder tissue. PGA has also been employed for bladder tissue

engineering. Stanasel *et al*. used a PGA-based scaffold for bladder augmentation in a canine model.[40] The results showed that the PGA scaffold could support the growth of bladder smooth muscle cells, leading to the formation of new bladder tissue. More examples are included in Table 2. However, the use of synthetic polymers also comes with challenges such as controlling the degradation rate to match tissue regeneration and enhancing bioactivity to support cell adhesion and tissue integration.

Table 1. Engineered biomaterials with different technologies for urinary tract reconstruction

Material Composition	**Fabrication**	**Advantages**	**Disadvantages**	**Experiments *in vitro* & *in vivo***	**Refs**
Collagen type I	Direct Bioprinting	• Radical elasticity • Great fatigue endurance	• Low elastic modulus • Low mechanical strength	*In vitro* SCaBER cells	[41]
GelMA + Alginate + PEGOA	Coaxial Extrusion	Tunable layer printing	Low mechanical strength	*In vitro* human bladder smooth muscle cells and urothelial cells	[42]
Autologous Tissue	Fused deposition modeling	Good 3D-printed anatomical statics and dynamics for posterior urethra	Limited grafts sources	N/A	[43]
PVA cryogel w/ PLA mold	Molding	Geometric, mechanical, and dynamic mimicry of urethra	Weak extensibility	N/A	[44]
PLA copolymer scaffold	Solvent Casting Particulate leaching	• Stable degradation profile • High porosity • Appropriate cell viability	Lack of cell-recognition sites	*In vitro* adult dermal fibroblasts	[45]
pre-seeding PGA/PLGA	Molding	• Tunable mechanical properties • great biocompatibility, no infections, and intraoperative complications upon implantation in human trial	Lack of cell-recognition sites	*In vivo* human trial	[46]

PEGOA, eight-arm poly(ethylene glycol); diacrylate PVA, poly(vinyl alcohol).

1.2 Microfabrication techniques used for urologic tissue reconstruction

1.2.1. Electrospun fibers

Electrospinning, a versatile fabrication technique, is widely utilized in tissue engineering due to its numerous advantages. The application of a high voltage to the polymer solution results in the creation of a charged jet. The solution in the syringe is forced out by the electrical force, which overcomes the surface tension of the liquid at the syringe tip. As the jet travels towards the collection plate, the solvent evaporates, and the polymer solidifies into fibers, which accumulate on the plate to form a non-woven mat.[47] During the process, the solution undergoes severe elongation and bending instabilities due to the electrostatic repulsion, creating thin, uniform fibers. Several parameters can be adjusted during the process to control fiber morphology, including solution properties (concentration, viscosity, conductivity), operational parameters (applied voltage, flow rate, tip-to-collector distance), and environmental conditions (temperature, humidity).[48] Electrospinning allows the creation of nanofibers from a wide range of polymers, both natural and synthetic. These fibrous scaffolds enable the production of scaffolds with a high surface-to-volume ratio, closely resembling the extracellular matrix of various tissues in terms of architecture and physical properties, which promotes cell attachment, proliferation, and differentiation.[49, 50] Furthermore, electrospinning allows for the incorporation of bioactive molecules, growth factors, and drugs into the polymer fibers, facilitating controlled release and improved regenerative potential. The adjustable properties of electrospun scaffolds, including fiber diameter, porosity, and mechanical strength, can be tailored to meet the specific requirements of urethral grafts. However, it is important to acknowledge certain limitations associated with electrospinning. The process can be challenging to control, resulting in variations in fiber morphology and alignment. Additionally, the use of organic solvents in electrospinning raises

concerns about cytotoxicity and biocompatibility. The mechanical properties of electrospun scaffolds may not always match those of native urethral tissue, necessitating additional reinforcement strategies. Despite these limitations, the advantages of electrospinning, such as the ability to produce bioactive nanofibrous scaffolds, make it a promising technique for urethral graft fabrication. Ongoing research focuses on optimizing electrospinning parameters, exploring novel polymer combinations, and integrating complementary technologies to address the limitations and enhance the functionality of electrospun urethral grafts.

Table 2. Different electrospinning methods used for urinary tract reconstructions

Material composition	Electrospinning method	Fiber diameter (nm)	Animal model	Outcomes	Refs
PLCL/HA	Coaxial-electrospinning	784.2 ± 138.2	*In vivo* Rat	Smooth muscle regeneration and increased bladder capacity	[51]
PCUU	Single-jet electrospinning	N/A	*In vivo* Rat (bladder outlet obstruction)	Increased voiding volume and caliculi formation	[52]
PEU/BAM	Double-jet electrospinning	3600 ± 300	*In vivo* Rat	Robust cell proliferation and spreading *in vivo*	[53]
PLGA/BAM	Single-jet electrospinning	4500 ± 250	*In vivo* Rat	Regeneration of bladder wall	[54]
Silk fibroin	Single-jet electrospinning	N/A	*In vivo* Rabbit	Restoration of tissue layers Mild acute and chronic inflammatory reactions	[55]
PLLA/PEG	Single-jet electorspinning	N/A	*In vivo* NZ White Rabbits, scaffolds with hAMSCs	Successful urethral defect repair	[56]
PLGA/collagen	Single-jet electorspinning	N/A	N/A	Improved urothelial cells attachment	[57]

PCL/PLLA	Double-jet electrospinning	120-1500	Dog	• excellent SMCs attachment • improved tissue regeneration	[58]

PLCL, poly (lactide-co-ε-caprolactone); PCUU, poly (carbonate-urethane) urea; PEU, poly (ester urethane); BAM, bladder acellular matrix; PLLA, poly (L-lactide) acid; PEG, polyethylene glycol; PCL, polycaprolactone.

1.2.2 3D bioprinting

3D bioprinting offers significant potential for engineering synthetic urethral tissue and addressing the current demand for solutions in this field. The limitations of current tabularized grafts often arise from the inability to replicate the diverse layers and highly extensible properties of native tissue. 3D bioprinting, with the ability to create constructs that replicate scanned patient anatomy, can provide specific benefits in this regard. Bioinks used in 3D bioprinting are typically hydrogels, which allow for easy manipulation of construct geometry through post-printing crosslinking reactions. This flexibility enables the selection of hydrogels and proteins as bioinks, offering a wide range of materials with desired mechanical properties for mimicking urethral tissue mechanics. By engineering 3D bioprinted constructs with appropriate materials, it becomes possible to create structures that closely resemble the mechanical properties of natural urethral tissue. While some bioprinting methods have already been applied to fabricate urethral constructs, as well as innovative biomimetic bioinks with tunable mechanical properties, there is still room for innovation in this field. Also, further *in vivo* examinations are required for most of the recently published works.[59, 60] Some techniques have focused on common tubular structures, but there is potential for exploring new approaches and materials to enhance the efficacy of urethral constructs. Each bioprinting technique has its own advantages and limitations, providing opportunities for novel studies that can further improve the engineering of urethral tissue constructs.

1.2.3 Molding

Molding is a method used to create versatile structures for urethral tissue reconstruction. This process involves knitting filamentary material membranes together and applying heat or pressure to bond them. This technique allows for adjustments to mechanical properties but has less precise control over texture compared to bioprinting. A key limitation is that it requires tissue from a patient which may result in longer processing times. Sartoneva et al. explored this technique, investigating how the texture of materials like PLA and PLCL affected the constructs. While all showed good stretchability, smooth PLCL lacked mechanical stability due to quick degradation.[61] Also, compound tubular grafts have been made using molding. Despite its applicability, other methods like electrospinning and 3D bioprinting may offer more advantages, such as direct reconstruction of damaged urethral areas and potentially simpler processes.[62]

1.3 Clinical gaps and project considerations for urinary tract reconstructions

Given the comprehensive literature review, it is evident that there are substantial clinical gaps and limitations with existing materials and technologies in urologic tissue engineering. The challenges range from insufficient tissue supply and the risk of host rejection to long-term stability and function of engineered tissues. Moreover, the biomaterials under investigation often exhibit inconsistent degradation profiles and sub-optimal mechanical properties, rendering them insufficient for clinical applications.

Among the diverse materials studied for tissue engineering, Gelatin Methacryloyl (GelMA), a functional derivative of collagen, stands out due to its superior biocompatibility, ease of synthesis, and cost-effectiveness. Its broad usage across various biomaterial applications, combined with its ability to be tuned in conjunction with other polymers, allows for the development of unique hydrogel systems with custom properties.

ELPs, on the other hand, are recognized for their stretchability, a property critical for urethral reconstruction. Incorporating electrospinning technologies, which aim to replicate the extracellular matrix's architecture, may pave the way for reconstructing urologic tissues using GelMA/ELP fibrous scaffolds. Hence, this potential combination offers a promising avenue for advancing urologic tissue engineering.

2. EXPERIMENTAL

2.1 Synthesis of biomaterials

2.1.1 Synthesis of gelatin methacryloyl (GelMA): GelMA was synthesized following a previously described method.[63] In summary, 20 g of gelatin (Sigma-Aldrich) sourced from cold water fish was dissolved in 200 mL of DPBS (Gibco) and heated to 100 °C until complete dissolution. Subsequently, 16 mL of methacrylic anhydride (Sigma-Aldrich) was gradually added to the gelatin solution drop by drop under vigorous stirring at 100 °C to modify the lysine groups on the gelatin chains. After 3 hours, to stop the methacrylation reaction, 400 mL of 100 ºC pre-heated DPBS was added to the solution. The solution was then dialyzed in dialysis tubes (Spectrum Laboratories, MWCO = 12-14 kDa) immersed in deionized water at 100 °C for 5 days to remove any unreacted methacrylic anhydride. After dialysis, the contents were frozen at -80 °C for at least 2 hours and subsequently lyophilized for 5 days to obtain the final GelMA product, which was stored at room temperature until further use in experiments.

2.1.2 Synthesis of elastin-like polypeptide (ELP): The photocrosslinkable ELP sequence was edited using a method previously described in our earlier study.[25] This kanamycin-resistant protein comprises 70 repetitions of the pentapeptide VPGVG, with an isoleucine substitution for the first valine every five pentapeptides, resulting in a pattern of $([VPGVG]4[IPGVG])_{14}$. To enable photocrosslinking through the formation of S-S thiol bonds, Lys-Cys-Thr-Ser (KCTS)

residues were incorporated on both sides of the ELP sequence. The ELP was expressed utilizing Escherichia coli (E. coli) as the host organism, followed by lysis and purification via inverse transition cycling, as previously reported.[64] The ELP solutions were then subjected to alternate equilibration and centrifugation above and below their thermal transition temperature (Tt = 29 °C in a 1% (w/v) solution). This temperature cycling takes advantage of the ELP solubility at low temperatures and precipitation at high temperatures, allowing for the removal of impurities and obtaining a pure ELP product. The purified ELP solution was subsequently dialyzed in a water bath at 4 °C against deionized (DI) water for 7 days following lyophilization until no weight change was observed.

2.1.3. Electrospinning of GelMA/ELP prepolymers: A prepolymer solution was prepared by dissolving different concentrations of GelMA (3, 5, 7, 10% (w/v)) and ELP (0, 3, 5, 7% (w/v)) in hexafluoroisopropanol solvent (HFIP) (Sigma-Aldrich) and placed in a 3 mL syringe with a 18G needle mounted on the pump. The prepolymer solution was pumped out at a constant rate of 1 mL/h. A high-voltage power supplier (Glassman High Voltage, Inc., Series EH) was attached to the needle of the syringe, and the voltage was set to 25 kV. A grounded metal collector was set 13 cm from the syringe nozzle. Then the fibrous scaffolds were placed in the desiccator overnight to remove any remaining solvent. The scaffolds were soaked in 1% (w/v) solution of Irgacure 2959 (Sigma-Aldrich) as a photoinitiator in ethanol for 2 hours and photo-crosslinked using UV light (6.9 mW/cm^2, EXFO OmniCure S2000) for 600 s. After repeated washing in DPBS, the hydrogel scaffolds were used for *in vitro* experiments.

2.2. *In vitro* characterization of biomaterial properties

2.2.1. ^{1}H NMR characterization of GelMA/ELP hydrogels: The degree of methacrylation of polymers such as GelMA have a well-established method of study, primarily

through quantifying the signals of free lysine proton nuclear resonance (^{1}H-NMR) groups with an increased degree of methacrylation.[46, 47] Providing a comparison for the area under these respective peaks within a crosslinked sample versus an uncrosslinked prepolymer solution was used to quantify the degree of crosslinking. 1cm x 1cm samples of both crosslinked and uncrosslinked 5E5G fibrous scaffold were dissolved in 1 mL dimethyl sulfoxide (DMSO-d_6) in 37 °C, before being prepared for study with ^{1}HNMR. ^{1}HNMR was performed using a 400 mHz Bruker AV400 spectrometer.

2.2.2. Scanning electron microscope (SEM): The morphologies of scaffolds were characterized by SEM (ZEISS Supra 40VP) at an accelerating voltage of 10 KV, with a magnification of 10,000 times. Before being characterized, the samples were mounted on SEM stubs and sputter coated with gold (SC7620, Quorum Technologies, UK).

2.2.3. Mechanical characterization: GelMA/ELP fibrous scaffolds were prepared as described before and cut to rectangular shape with a replacement blade. The rabbit urethral, bladder and foreskin tissues in DPBS were obtained from the UCLA urology department. The dimensions of the hydrogels and tissues were then measured using a caliper. An Instron 5943 mechanical tester was used to perform tensile and cyclic tensile tests. For the tensile test, hydrogels and tissues were fixed between two pieces of double-sided tape which were held between two tension grips and stretched at a rate of 1 mm/min until failure. The tensile strain (mm) and load (N) were recorded using the Bluehill software. Young's modulus was calculated as the tangent slope of the stress−strain curve. Cyclic tests (10 cycles/sample) were performed at maximum 150% strain and a rate of 1.5 %/s by performing 10 cycles of loading and unloading. The tensile strain (mm) and load (N) were measured using the Bluehill software. Cycle 8 was picked as the representative

curves for both hydrogels and tissues. Energy loss was calculated by obtaining the area between the loading and unloading curve for cycle 8 (n = 5).

2.2.4. Suture retention test: GelMA/ELP fibrous scaffolds and were prepared as described in section 2.1.3. Rabbit urethral tissues were obtained from the UCLA urology department. An Instron 5943 mechanical tester was used to perform suture retention test. Different from the traditional suture retention test by Smitten et al., the two selected grafts were completely sutured together (add ref here). For suturing scaffold to scaffold, the suture was placed 2 mm from the sides of the two scaffolds. The same procedures were applied when suturing scaffolds to urethral tissues. Scaffolds and tissues were fixed between two pieces of double-sided tape which were held between two tension grips and stretched at a rate of 1 mm/min. The endpoint was determined when the scaffolds were severed from the sutures (See Fig. 3C). The rupture stress was recorded (n=4).

2.2.5. *Ex vivo* sealing test: The pressure required to rupture/detach the graft from the *ex vivo* rabbit bladder model was measured using at least 3 bladders and grafts per condition. A circular defect (diameter = 3 mm) was made on the bladder using a surgical scissor, and a 1 cm x 1 cm graft was applied onto the defect, and the PDS II suture of size 6-0 was used to sutured around the defect to seal it with a taper point needle. The bladder was gradually filled with DI water at a constant rate of 5 mL min^{-1} using a single syringe pump, and the pressure was monitored using the *in vitro* burst pressure setup. The burst pressure was defined as the maximum pressure at which water started leaking from the sealed defect, resulting in dropped or plateaued pressure. The graft materials used were 0E10G fibrous scaffolds, 5E5G fibrous scaffolds, SIS scaffolds, bladder and bowel tissue. Rhodamine b (Sigma-Aldrich) was added to water as a color indicator, enhancing the visual detection of the leakage.

2.2.6. *In vitro* degradation: 5 mm in diameter circular samples were created by a biopsy puncture (n = 3). The samples were placed in small vials, lyophilized, weighed, and recorded as initial weight W_0 at 0 h. Then the samples were incubated until completely degraded at 37 ^oC in 0.5 mL of DPBS , 0.5 mL of 0.1U/mL of DPBS-porcine elastase solution, 0.5 mL of 1.5U/mL of DPBS-type I collagenase solution, and the mixture solution of 0.25 mL of 0.1U/mL of DPBS-porcine elastase solution and 0.25 mL of 5U/mL of DPBS-type I collagenase solution, repectively. At day 1, 2, 4, 7, 10, 14, 21, 28, (day 30, 38, 40 based on the ending point), and complete degradation, the samples were retrieved, lyophilized, and weighted. The incubation solution was replaced every 3 days. The percentage degradation (D%) of the hydrogels was calculated using the below equation:

$$D\% = \frac{W_t - W_0}{W_0} \times 100 \qquad \textbf{(1)}$$

where W_0 is the initial dry weight of the sample and W_t is the dry weight at time t.

2.2.7. Swelling ratio measurements: The equilibrium swelling ratios of GelMA/ELP scaffolds were evaluated. For this purpose, 5 mm in diameter circular-shaped hydrogels were prepared as previously described in section 2.2.6 (n=3). Prepared scaffolds were washed with DPBS, lyophilized, and weighed. Then the samples were immersed in DPBS at 4, 37 ^oC and room temperature for 1, 2, 4 and 8 h (until no increase in weight was observed) and weighed again after immersion. The swelling ratio (SR%) of the hydrogels was calculated using the below equation:

$$\mathrm{SR}\% = \frac{W_s - W_0}{W_0} \times 100 \qquad \textbf{(2)}$$

where W_0 is the initial dry weight of the sample and W_s is the swelling weight of the sample at time t.

2.2.8. Surface seeding (2D culture): SMCs (ATCC PCS-420-012) (10^4 cells/scaffold) were seeded on the surface of the hydrogels and placed in 24-well plates with 1000 µL of growth

medium (ATCC PCS-100-030) to each well. 2D cultures were maintained at 37 ºC in a 5% CO_2 humidified atmosphere, for 7 days and culture medium was replaced every 48h. The surface seeding process of urothelial cells was similar to that of SMCs. Urothelial cells (ATCC PCS-420-010) (10^4 cells/scaffold) were seeded on the surface of the hydrogels and placed in 24-well plates with 1000µL of growth medium (ACTT PCS-420-042) to each well.

2.2.9. Cell viability: The viability of SMCs grown on the surface of GelMA and GelMA/ELP scaffolds were evaluated using a commercial live/dead viability kit (Invitrogen), according to instructions from the manufacturer. A solution of stain was made by adding 1 mL of Calcein, AM cell permeant dye (live indicator) to 1µL of BOBO-3 Iodide (dead indicator). After thoroughly mixing, 50 µL/mL of staining solution was added to each well containing cells and incubated at room temperature for 15 minutes before imaging. Fluorescent image acquisition was carried out at days 1, 5, and 7 post-seeding using an Evos M5000 (Initrogen by Thermofisher). Viable cells appeared as green and apoptotic/dead cells appeared as red. The number of live and dead cells was quantified using the ImageJ software. Cell viability was determined as the number of live cells divided by the total number of live and dead cells. The staining, characterization and quantification process of urothelial cells were the same as that of the SMCs.

2.2.10. Metabolic activity: The metabolic activity of the cells was evaluated at days 1, 3, 5 and 7 post-seeding, using a PrestoBlue assay (Life Technologies) according to instructions from the manufacturer. Briefly, 2D cultures of SMCs were incubated in 1000 µL of growth medium with 10% PrestoBlue reagent for 1 h at 37 ºC. After 1hr, 100µL aliquots of 10% presto blue that had been incubated with cells were pipetted into 4 wells in a 96-well plate. The resulting fluorescence was measured (excitation 540 nm; emission 600 nm) using a Synergy HT fluorescence plate reader (BioTek). Control wells without cells were used to determine the

background for all experiments. The same procedures were applied to determine the metabolic activity of urothelial cells.

2.2.11. Cell adhesion, proliferation and spreading: SMCs spreading on the surface of the engineered scaffolds were visualized through fluorescent staining of F-actin 54 filaments and cell nuclei. Briefly, 2D cultures at days 1, 5, and 7 post-seeding were rinsed twice for 5 min/rinse with 1 mL DPBS, fixed in 4% (v/v) neutral buffered formalin (Epredia) for 15 min., rinsed twice at 5 min/rinse with 1 mL DPBS, and permeabilized in 0.1% (w/v) Triton X 100 (Sigma) for 15 min. After permeabilization, samples were rinsed 2 times for 5 minutes with 1mL of DPBS. 1mL of DPBS was added to the sample after the last rinse and 2 drops/mL of ActinRed TM 555 ReadyProbes TM reagent (Rhodamine phalloidin) (Thermofisher) were added to each well. The samples were incubated in actin stain for 30 minutes and 2 drops/mL of NucBlue TM Fixed Cell ReadyProbes TM Reagent (DAPI) (Thermofisher) were added to each sample and incubated for another 30 min. Fluorescent imaging was carried out using the Evos M5000 (Invitrogen). The same procedures were applied to urothelial cells.

2.2.12. Statistical analysis: The reported data consist of the mean values derived from a minimum of three replicates, along with their respective standard deviations. The statistical analysis was conducted via a two-way ANOVA, followed by a post-hoc Tukey's multiple comparison test, utilizing the GraphPad Prism software (version 8.2.1). The level of statistical significance was indicated as follows: * for $p < 0.05$, ** for $p < 0.01$, *** for $p < 0.001$, and **** for $p < 0.0001$.

3. RESULTS AND DISCUSSION

3.1. Synthesis and fabrication of GelMA/ELP fibrous scaffolds

Hybrid hydrogels have been developed with the aim of optimizing the mechanical properties, diffusion rate, and biological activities of incorporated therapeutic molecules, rendering them well-suited for intended medical applications.[65] Moreover, in contrast to hydrogels with a single polymer network, hybrid hydrogels exhibit greater capacities to emulate versatile properties of native physiological microenvironments.[66] GelMA and ELP can be microfabricated to better resemble the composition, morphology and some other essential properties of native ECM, thereby facilitating cell proliferation and spreading within GelMA-based scaffolds. In addition, tunable physical characteristics enable GelMA to become widely used in tissue engineering applications.[67] The genetically encoded synthesis provides complete control over the amino acid sequence and molecular weight and other physicochemical properties of ELPs, allowing for their wide-ranging utilization in biomedical applications where stretchability is of main importance.[68-70] Despite the excellent inherent bioactivates of GelMA-based hydrogels, their poor elasticity and suturability have limited their clinical applications in urological tissue reconstructions.[71] Therefore, it is plausible to postulate that the incorporation of highly elastic ELPs into GelMA-based hydrogels could effectively increase the elasticity and resilience of the hydrogel system upon photocrosslinking.

Here, we engineered a hybrid hydrogel based on GelMA and ELP to electrospun elastin and suturable scaffolds for urethra reconstruction. In this regard, GelMA was synthesized by adding methacrylic anhydride to gelatin derived from cold water fish due to its better solubility at 4 °C compared to gelatin from porcine (**Figure 1a**).[72] Following that, a highly elastic photocrosslinkable ELP was successfully synthesized and purified using a methodology detailed in our prior study.[25] ELP used in this study possesses a carefully engineered sequence that has been experimentally validated to exhibit enhanced mechanical properties, characterized by

remarkable stretchability, along with notable structural stability. Moreover, the strategic inclusion of cysteine residues at both ends of the protein sequence enables efficient photocrosslinking (**Figure 1b**). To prepare GelMA/ELP prepolymer, different concentrations of GelMA (ranging from 3% to 10% (w/v)) and ELP (ranging from 0% to 7% (w/v)) were combined and dissolved in HFIP at room temperature. Then the electrospun scaffold was collected in an aluminum collector following the formation of the fibrous scaffold by crosslinking with a 1% (w/v) solution of Irgacure 2959 as a photoinitiator upon exposing to UV light for 600 s (**Figure 1c**). Upon being subjected to UV radiation, the methacrylate moieties within GelMA interacted with the thiol (-SH) groups present in the cysteine residues of the ELPs, as well as underwent self-reaction. This resulted in prompt photocrosslinking and the creation of a 3D hydrogel framework that provides a suitable 3D environment for endothelialization and has great potential in tissue engineering (**Figure 1d**).[25, 73, 74] The effectiveness of the crosslinking process was demonstrated by observing the insolubility of the crosslinked scaffold when placed in an aqueous solution. SEM images showed that the matrices formed highly porous and non-woven mats of fibers with sub-micrometer diameters (**Figure 1e**). The average diameters of 0E10G fibers were approximately 660 nm and those of 5E5G were approximately 400 nm (**Figure 1e**). Analysis of the ^{1}HNMR spectra for uncrosslinked systems indicated the presence of peaks corresponding to methacrylate and methacrylamide groups at approximately 5.3 and 5.7 parts per million (ppm) respectively (referred to as b and c in **Figure 1f**). The chemical environments of the H protons in these groups are distinct due to the presence of double bonds, resulting in expected peak splitting. However, in crosslinked samples, these peaks were significantly reduced in intensity, providing evidence of successful linkages. These findings align with previous studies on GelMA and ELP.[75]

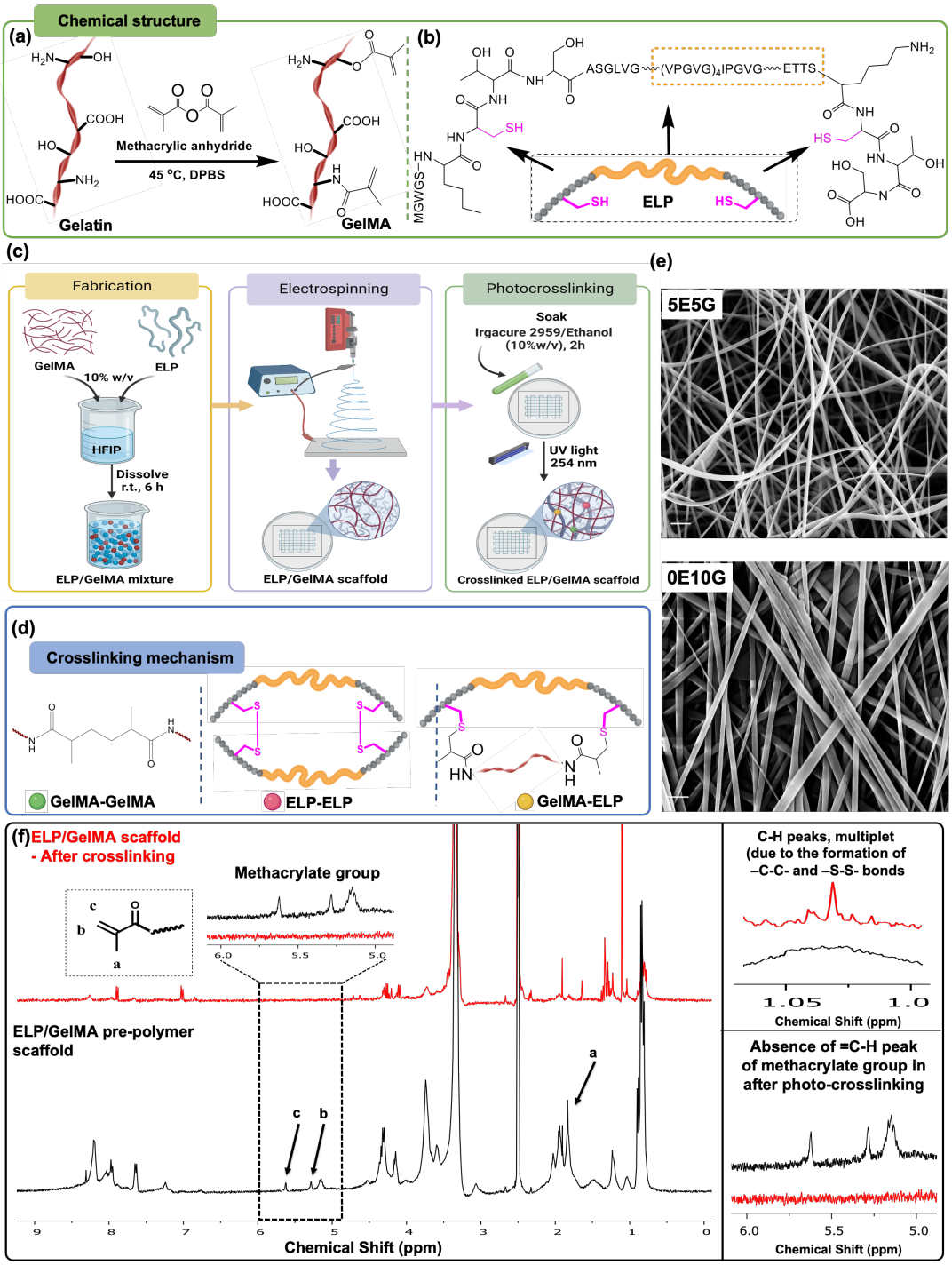

Figure 1. Schematic of GelMA/ELP fibrous scaffold formation and chemical structure. (a) Gelatin methacrylation to form GelMA; (b) Chemical structure of ELP, indicating the presence of thiol group, (c) GelMA/ELP hydrogels formation schematic diagrams including fabrication, and

(d) Different crosslinking mechanism, (e) Representative SEM images of a 5% GelMA and 5% ELP hydrogel (5E5G) and a 10% GelMA hydrogel (0E10G). (f) A representative NMR shows successful crosslinking.

3.2. Mechanical characterization of the GelMA/ELP fibrous scaffolds

Mechanical properties including the stiffness and elasticity of the ECM play an important role in governing numerous cellular processes and facilitating the development of new urologic tissues.[76, 77] With new insights into the influence of mechanical properties on cell behavior, we aimed to characterize and evaluate the mechanical properties of the engineered hydrogels synthesized with different concentrations of GelMA (i.e., 3, 5, 7 and 10% (w/v)) and ELP (i.e., 0, 3, 5, 7% (w/v)) by performing tensile and cyclic tensile tests (**Figure 2**). By varying the composition concentration percentage of GelMA and ELP, the tensile tests conducted on GelMA/ELP revealed their tunability on Young's modulus, ultimate strength (ultimate stress), and extensibility, with a subsequent comparison to the mechanical properties of native urethral and bladder tissues in adult male rabbits (**Figure 2a-c** and **Figure S1a-c**). The results show that the engineered hybrid hydrogels at a fixed final polymer concentration of 10% exhibited Young's modulus in the range of 12.44 ± 4.24 kPa to 25.63 ± 4.77 kPa for hydrogels with different ratios of GelMA and ELP concentration while the native rabbit urethral and bladder exhibited Young's modulus of 58.89 ± 16.54 kPa and 153.6 ± 468.67 kPa, respectively. There is no significant difference in Young's modulus observed between the native tissues and the four composition hybrid hydrogels. In particular, hydrogels synthesized with 5% ELP and 5% GelMA exhibited the highest Young's modulus (i.e., 25.63 ± 4.77 kPa) (**Figure 2a**). The results also showed that the ultimate strength of the engineered hydrogels increased from 19.43 ± 3.08 kPa to 27.48 ± 5.32 kPa when the concentration of GelMA increased from 3% to 10% (w/v). However, among the hydrogels

synthesized, those composed of 5% ELP and 5% GelMA displayed the highest ultimate strength (40.96 ± 6.68 kPa), exhibiting no significant difference from the ultimate strengths of rabbit urethral tissues (99.82 ± 24.14 kPa) and bladder tissues (138.9 ± 40.6 kPa) (**Figure 2b**). Lastly, mechanical characterization of GelMA/ELP hydrogels demonstrated significantly higher extensibility when fabricated with higher concentrations of ELP with a maximum strain reaching 168.3 ± 11.7%. In comparison, the extensibilities of urethral and bladder tissues were 322.6 ± 75.5 kPa and 194.5 ± 21.35 kPa, respectively (**Figure 2c**). Several theories have been proposed to elucidate the mechanism underlying the elasticity of elastin protein. One hypothesis suggests that when the polymer is stretched, the hydrophobic groups within the chain become exposed to the outer environment. This extension of the protein leads to an overall increase in the system's energy, and the recoil of elastin is driven by enthalpic forces. Alternative theories focus on the interplay between hydrophobic and hydrophilic groups to account for the elasticity observed in elastin.[78] The mechanical properties of urological tissues vary substantially depending on the maturity of the organism, composition and organization of ECM, the development of disease, as well as during physiological compression, tension, and shear stress.[79, 80]

Hence, for urological tissue engineering, it is crucial for the scaffolds to exhibit exceptional adjustability in terms of their mechanical properties to attain significant clinical applicability. The results clearly showed that by combining various concentrations of GelMA and ELP, hydrogels with a diverse array of extensively adjustable mechanical properties could be achieved. Consequently, the incorporation of these two biopolymers bestowed the hybrid hydrogels with an extraordinary capacity for tunability, making them extremely promising biomaterials for fabricating urological tissue constructs with tailored mechanical characteristics.

The cyclic tensile testing of the hybrid hydrogels demonstrated favorable recoverability of the gel even after multiple stretching cycles (**Figure 2d** and **Figure S1e**). The energy loss, measured during the eighth cycle, was determined to be 44.86 ± 15.63% for the ELP/GelMA hydrogels, while rabbit urethral tissues exhibited an energy loss of 29.09 ± 6.95% under the same conditions (**Figure 2e**). The relatively low energy dissipation observed during the loading and unloading cycles, coupled with the high resilience of GelMA/ELP hydrogels, underscores their potential for applications in urinary tract reconstruction.

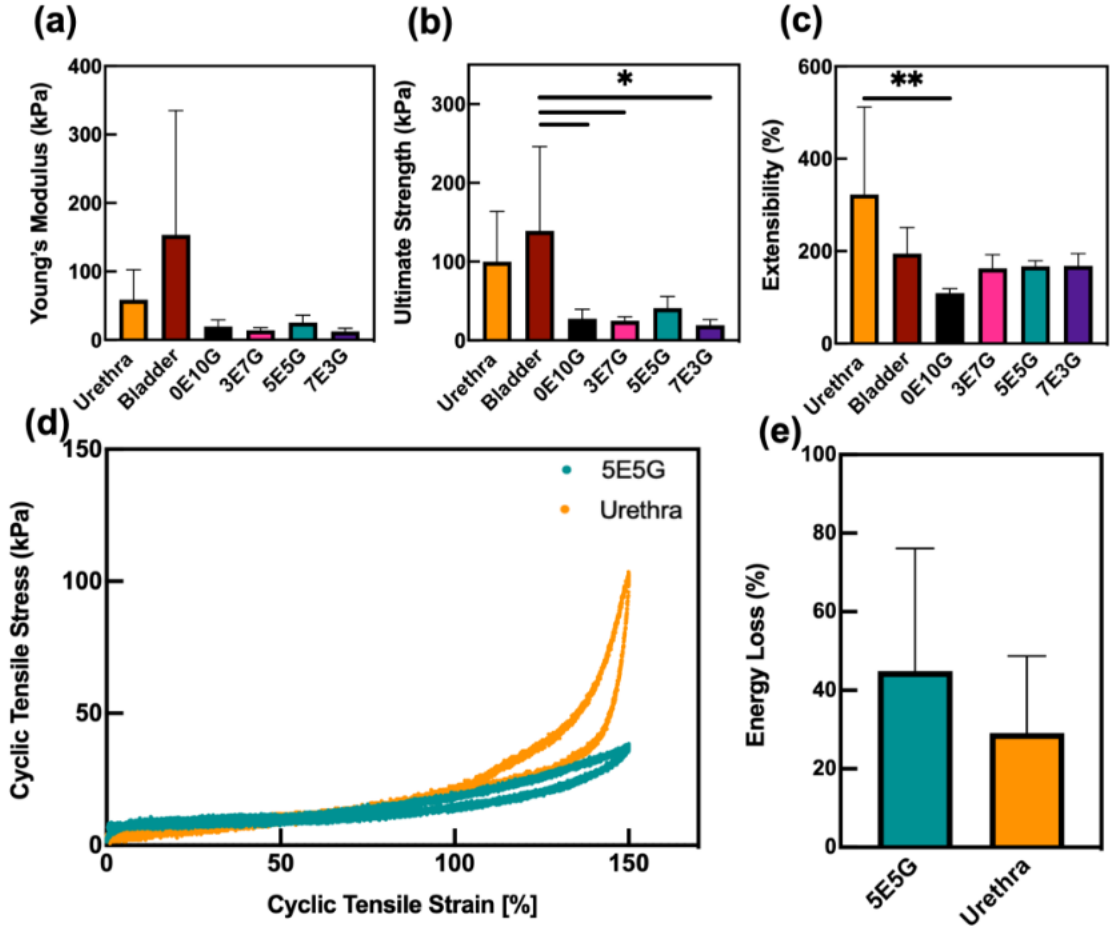

Figure 2. Mechanical properties of photocrosslinkable GelMA/ELP fibrous scaffolds compared to adult male rabbit urethra and bladder tissue. (a) Tensile Young's modulus, (b) Ultimate strength, and (c) Extensibility of rabbit tissues and different ratios of GelMA/ELP scaffolds, (d) Representative 8th cycle tensile curve of rabbit urethral tissue and GelMA/ELP scaffolds (5% GelMA and 10% ELP), (e) Energy loss of rabbit urethral tissue and GelMA/ELP

scaffolds (5% GelMA and 5% ELP) during 10 cycles cyclic test. (* $p < 0.05$, ** $p < 0.01$, *** $p < 0.001$, **** $p < 0.0001$).

3.3. Suture retention testing and *ex vivo* sealing capability of the scaffolds

It is necessary to carefully study the strength of the engineered hybrid scaffold when it is in contact with the suture line because most early graft failures are due to rupture of the graft to native tissue anastomosis.[81] The suture processes were shown in **Figure 3a** and **b**. The ability of GelMA/ELP fibrous scaffolds to withstand forces resulting from suturing was measured by suture retention strength, which was assessed by applying a controlled force to the suture until it fails as shown in **Figure 3c**. When ELPs were incorporated into the hydrogel networks, the suture retention strength of the GelMA/ELP electrospun scaffolds significantly increased. The suture retention strength improved from 9.62 ± 2.75 kPa to 14.62 ± 5.47 kPa for scaffold-to-scaffold suturing and from 7.42 ± 1.95 kPa to 13.29 ± 1.49 kPa for scaffold-to-tissue suturing. In addition, there is no statistically significant difference in suture retention strength observed between scaffold-to-scaffold suturing and scaffold-to-tissue suturing for both 0E10G and 5E5G scaffolds (**Figure 3d**).

To simulate the sealing of stretchable organs, we conduct *ex vivo* sealing experiments on rabbit bladders. An *ex vivo* rabbit bladder underwent a manual perforation, followed by the suturing of grafts and filling with DI water at a constant rate. In contrast to SIS, although GelMA/ELP scaffolds were not able to withstand as much burst pressure, they exhibited the ability to stretch in tandem with bladder tissues without causing any disruption to the shape of the bladder tissues (**Figure 3e**). The composition of hybrid hydrogels has a direct effect on the burst pressure that the sealed bladder could withstand. The 0E10G scaffold sealant provided a burst pressure of 2.12 ± 0.22 mmHg, which increases to 3.75 ± 0.36 mmHg by increasing the ELP concentration to 5% (**Figure 3f**). The effect of GelMA/ELP composition on the *ex vivo* burst pressure is similar to that on the tensile strength. Moreover, the sealing abilities of grafts that are currently used for clinical

urological surgeries were also tested under the same condition and compared to those of GelMA/ELP hybrid hydrogels. No statistically significant differences in sealing abilities were observed in bladder tissues, SIS and GelMA/ELP scaffolds. However, bowels, the lower opening of the digestive tract, showed significantly higher sealing abilities than those of 0E10G and 5E5G scaffolds.

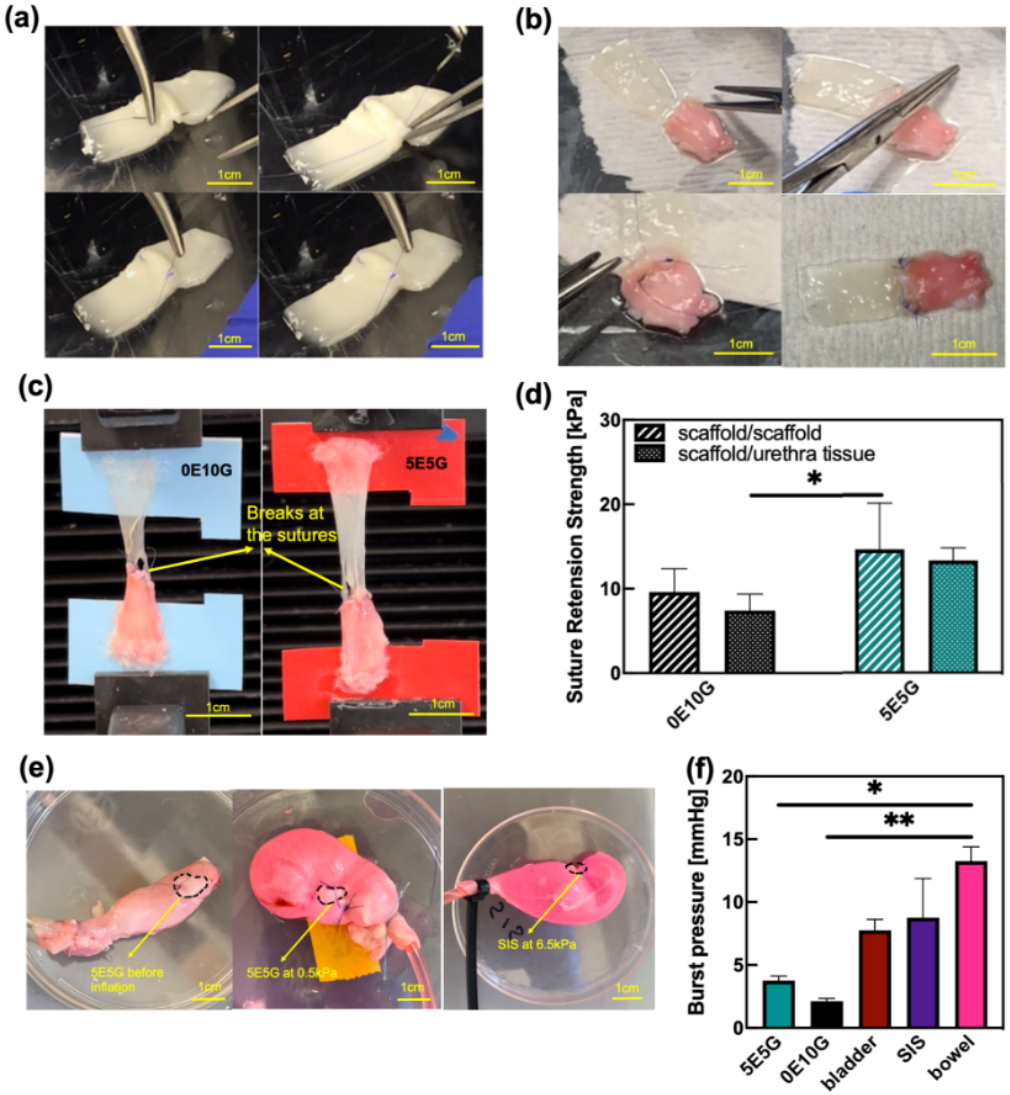

Figure 3. Suturability and *ex vivo* burst pressure of photocrosslinkable GelMA/ELP fibrous scaffolds compared to current grafts in clinical practice. (a) Sutured GelMA/ELP scaffolds together, (b) Sutured GelMA/ELP to rabbit urethral tissue, (c) Illustrative of suture breakage during stretching, (d) Ultimate suture retention strength of GelMA/ELP at different concentrations, urethral tissue and SIS, (e) Illustration of *ex vivo* burst pressure rabbit bladder model, (f) Observed

pressure when the suture on rabbit bladder model is ruptured or leaked (* $p < 0.05$, ** $p < 0.01$, *** $p < 0.001$, **** $p < 0.0001$).

3.4 *In vitro* swelling behavior and degradation rates of GelMA/ELP fibrous scaffolds

Hydrogels, known for their high hydrophilic properties, are primarily composed of water.[82] However, excessive water uptake can potentially weaken the interaction between polymer chains, leading to reduction in the mechanical properties of engineered scaffolds.[83] Moreover, rapid, and excessive swelling rates of implanted scaffolds can lead to significant morphological changes and the risk of compressing nerves and surrounding tissues.[84] Therefore, the evaluation of water uptake capacity in GelMA/ELP fibrous hydrogels was a key objective of our study.

Our results indicated that both 0E10G and 5E5G scaffolds exhibited rapid swelling within 1 hour of incubation at 4, 25, and 37 °C. However, there were no significant increases in water uptake observed after 4 hours of incubation for all tested samples (**Figure 4c-d**). Additionally, hydrogels with higher ELP concentrations demonstrated lower swelling compared to those with lower ELP concentrations. This can be attributed to the highly hydrophobic repeating motifs ([[VPGVG]4IPGVG]14) present in the chemical structure of ELP.[85] The hydrophobic interactions, combined with an increase in ELP concentration, likely led to higher crosslinking density, resulting in decreased swelling ratios.[25] Furthermore, no significant difference in the swelling ratio of 0E10G was observed with changes in incubation temperature, whereas 5E5G showed significantly higher swelling at 4°C compared to higher temperatures.

For clinical applications, it is imperative that designed polymeric networks degrade into non-toxic byproducts while allowing sufficient time to facilitate autologous tissue regeneration. This strategy ensures that the advantageous outcomes associated with scaffold use are not compromised by potential adverse effects induced by scaffold degradation.[86, 87] In an effort to replicate the urinary

tract microenvironment more precisely, degradations of different composites of GelMA/ELP scaffolds (0E10G, 3E7G, 5E5G, and 7E3G) were characterized in the presence of elastase and collagenase at 37 ºC until the scaffolds were completely degraded (**Figure 4a-b**, **Figure S1g-h**). These enzymes are inherent to the urinary tract and play a critical role in the disassembly and remodeling of ECM proteins, including those integral to bioactive scaffolds. [88] This helps to ensure that the degradation rate of the scaffold aligns with the natural regeneration rate of the tissue and that the scaffold material doesn't lead to any unwanted build-up in the body.[29] As anticipated, scaffold degradation rates in collagenase solutions increased in line with GelMA concentrations, while in elastase solutions, rates increased with ELP concentrations (**Figures 4a-b**, **S1g-h**). Our results demonstrated that the degradation rates of the engineered hydrogels can be moderately slowed with higher ELP compositions. The weight loss of varying composition scaffolds was evaluated at specified intervals in PBS solutions (**Figure 4e**), revealing a decrease in scaffold weight loss with increased ELP compositions. Interestingly, the 5E5G scaffolds exhibited the least weight loss in both collagenase and elastase presence while when the ELP concentration reached 7% (w/v), the scaffolds experienced greater weight loss than those with lower ELP compositions (**Figure 4f**). This can be attributed to the optimal compositions of GelMA and ELP facilitating additional physical crosslinks and complex polymeric networks. Given that elastase generally degrades elastin faster than collagenase degrades collagens under identical conditions,[89] a high ELP concentration can lead to accelerated scaffold degradation if the elastase activity outpaces the ELP resistance. The presence of enzymes also significantly increased scaffold degradation rates. Scaffolds with ELP compositions of 0, 3, 5, and 7% (w/v) were entirely degraded in PBS after 38, 39, 41, and 45 days, respectively. In contrast, all scaffolds were fully degraded in mixed elastase and collagenase solutions within 7 days. Overall, these findings suggest that GelMA/ELP fibrous

scaffolds exhibit controllable degradation and have the potential of being safely removed from the physiological environment post-implantation.

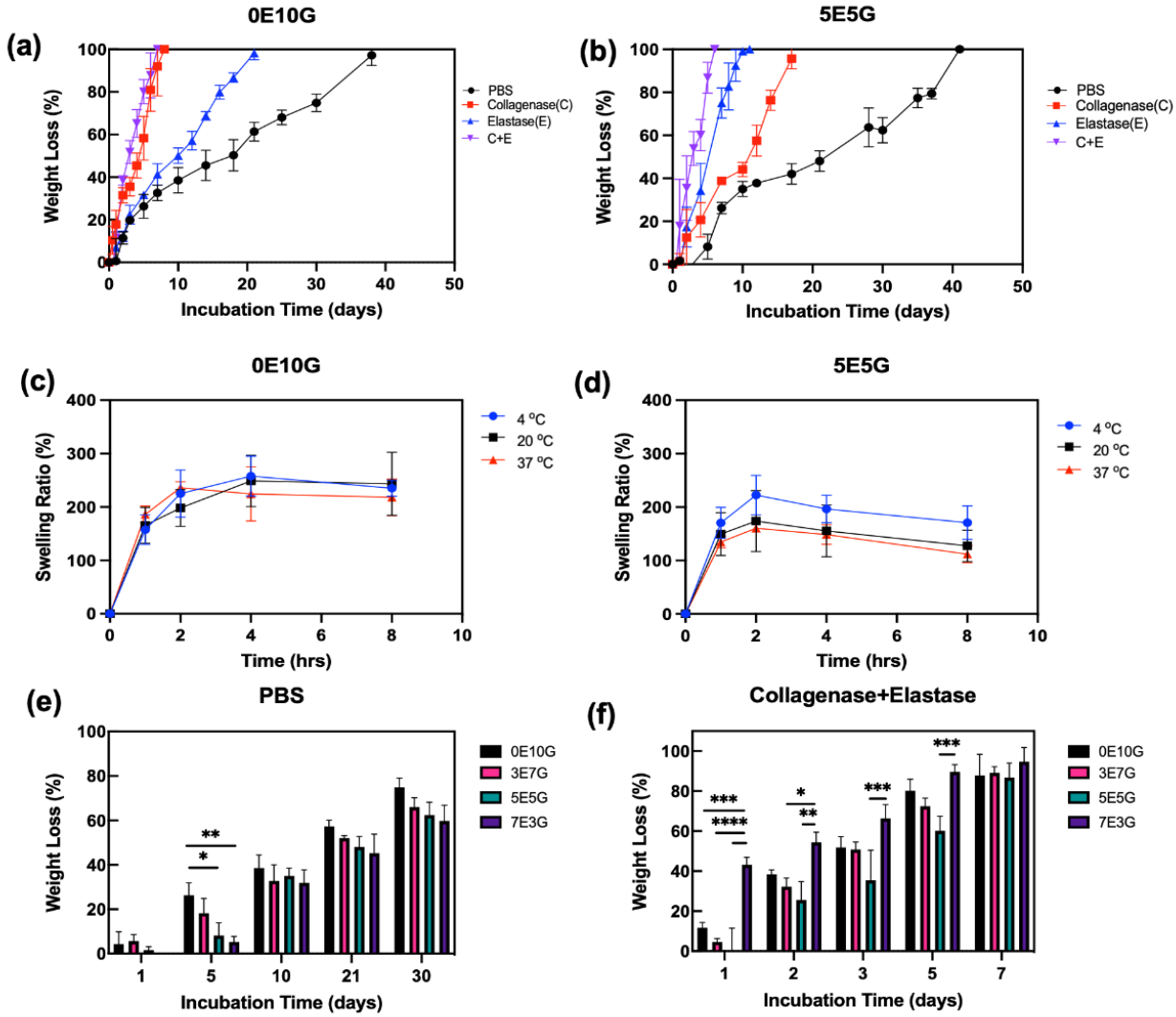

Figure 4. Biodegradation and swelling behavior at different concentrations. Degradation profile for (a) 0E10G and (b) 5E5G with and without collagenase and elastase, Swelling ratios of (c) 0E10G and (d) 5E5G scaffold at 4, 20 and 37 °C. Comparisons of the degradation profiles of varies compositions of GelMA/ELP scaffolds (0E10G, 3E7G, 5E5G and 7E3G) at selected time points in (e) PBS and (f) the collagenase and elastase mixtures. (* $p < 0.05$, ** $p < 0.01$, *** $p < 0.001$, **** $p < 0.0001$).

3.5 *In vitro* evaluation of the cytocompatibility of GelMA/ELP fibrous scaffolds

Bioactive scaffolds offer structural reinforcement in tissue reconstruction processes. Also, they play a crucial role in modulating cellular behaviors in multiple ways.[90] The scaffold composition

promotes initial cell attachment, a prerequisite for cell proliferation.[31] Additionally, their porous architecture supports cell migration, tissue formation, and essential nutrient and oxygen exchange.[91, 92] Moreover, scaffold mechanical properties can affect cell phenotype and functions via mechanical signal transduction.[93] To more accurately mimic the urethral cellular environment which comprises an inner urothelial layer and a smooth muscle layer within the urethral wall, three cell lines—SMCs (ATCC PCS-420-012) (Figure 5), urothelial cells (ATCC PCS-429-010) (**Figure 6**), and fibroblasts (ATCC BJ-CRL-2522) (Figure S2)—were utilized.[94] The viability, proliferation, and adhesion of these cell lines in the 5E5G and 0E10G scaffolds were assessed through commercial live/dead and PrestoBlue assays, alongside Actin/DAPI fluorescent staining. The results revealed that both engineered hydrogel scaffolds exhibited excellent cell survival for all three cell lines up to 7 days post-seeding (**Figure 5a-d**, **Figure 6a-d**, and **Figure S2a-d**) with >90% cell viability (**Figure 5e**, **Figure 6e**, and **Figure S2e**). Moreover, the increased fluorescent intensities on the scaffolds in Figure 5f-i and Figure S2f-i showed that both 5E5G and 0E10G support cell proliferation, spreading and adhesion throughout the duration of the experiment for both SMCs and fibroblast cells. However, it appeared a decreased fluorescent intensity on both scaffolds during the experiment period. Due to inherent cell-to-cell adhesion mechanisms, urothelial cells typically grow closely together, forming a continuous, cohesive layer integral to their barrier function within the urinary tract.[95] Given this preference for attachment, we hypothesize that the existing pore sizes of the scaffolds may not sufficiently accommodate the growth of urothelial cell aggregates within them. Lastly, the metabolic activity increased rapidly (>3-fold) for both scaffolds the first 5 days post-seeding as cells reached maturity for SMCs (**Figure 5j**) and fibroblast cells (**Figure S2j**). Given the distinct biological characteristics and roles of various cell types, their proliferation rates can differ markedly. Specifically, urothelial cells

exhibit a slower turnover rate compared to fibroblast and smooth muscle cells, as their normal physiological functions do not necessitate rapid proliferation, leading to their inherently slower growth.[96] The metabolic activity data (**Figure 6j**) indicated a consistent increase in urothelial cell activity throughout the experimental duration for both the 5E5G and 0E10G fibrous scaffolds. In summary, the results indicate that GelMA/ELP fibrous scaffolds exhibit superior biocompatibility, suggesting their potential utility in supporting *in vivo* tissue repair.

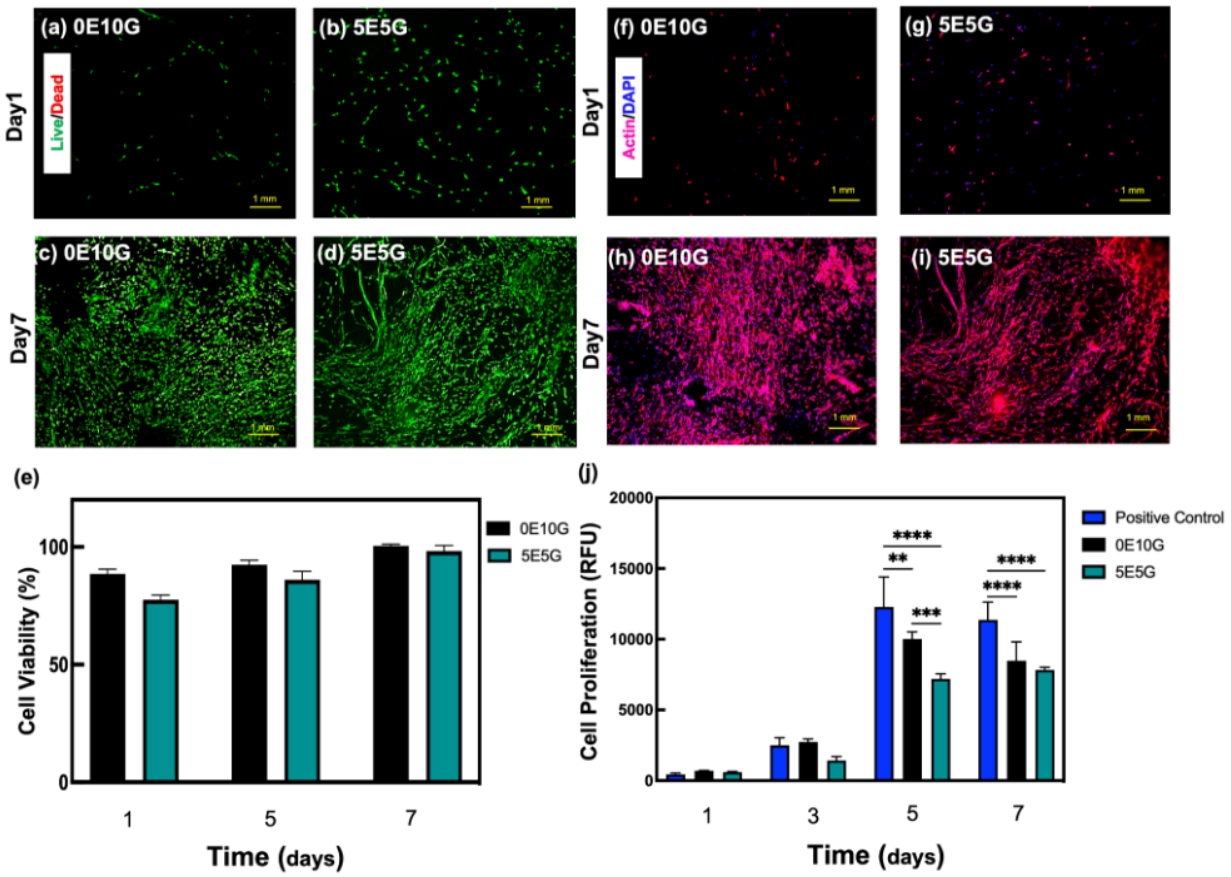

Figure 5. *In vitro* cytocompatibility of GelMA/ELP fibrous scaffolds using SMCs. Representative live/dead images from SMCs seeded on (a) 0E10G and (b) 5E5G scaffolds at day 1, and representative live/dead images from SMCs of seeding on (c) 0E10G and (d) 5E5G scaffolds. Quantification of (e) viability after 1, 5 and 7 days of culture. Representative Actin (red)/DAPI (blue) stained images from SMCs seeded on (f) 0E10G and (g) at day 1 and representative Actin (red)/DAPI (blue) stained images from SMCs seeded on (h) 0E10G and (i) at day 7 post culture. Quantification (j) metabolic activity of SMCs seeded on scaffolds after 1, 3, 5 and 7 days of culture. (* $p < 0.05$, ** $p < 0.01$, *** $p < 0.001$).

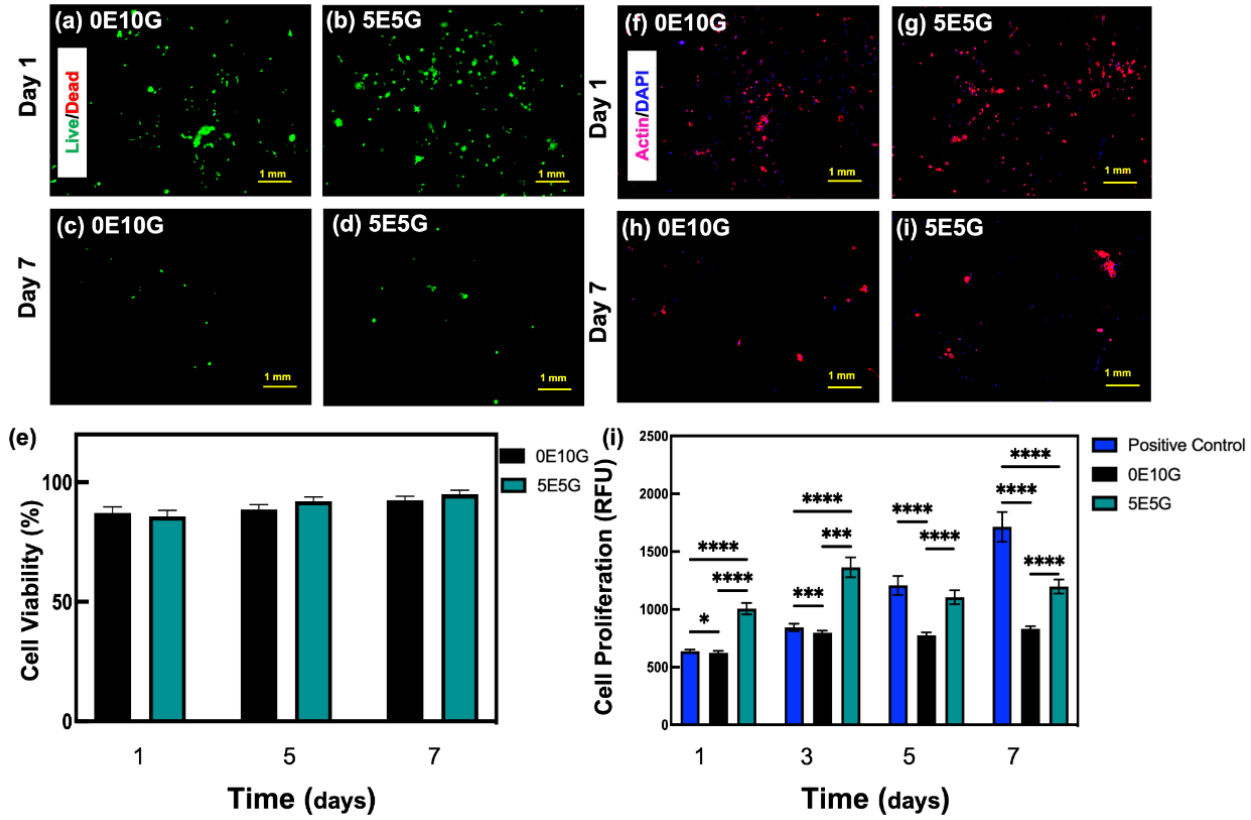

Figure 6. ***In vitro*** **cytocompatibility of GelMA/ELP fibrous scaffolds using urothelial cells.** Representative live/dead images from urothelial cells seeded on (a) 0E10G and (b) 5E5G scaffolds at day 1, and representative live/dead images from urothelial cells of seeding on (c) 0E10G and (d) 5E5G scaffolds. Quantification of (e) viability after 1, 5 and 7 days of culture. Representative Actin (red)/DAPI (blue) stained images from urothelial cells seeded on (f) 0E10G and (g) at day 1 and representative Actin (red)/DAPI (blue) stained images from urothelial cells seeded on (h) 0E10G and (i) at day 7 post culture. Quantification (j) metabolic activity of urothelial cells seeded on scaffolds after 1, 3, 5 and 7 days of culture. (* $p < 0.05$, ** $p < 0.01$, *** $p < 0.001$).

4. CONCLUSION

In this thesis, we first introduced the current potential biomaterials, technologies and facing challenges for urologic tissue engineering. Then we engineered suturable elastic GelMA/ELP fibrous scaffolds with tunable mechanical strength, elasticity, degradability, and swellability by varying the polymer compositions. For example, the elasticity can be enhanced and the degradation rate can be lowered by increasing the ELP concentrations. Additionally, the engineered scaffolds exhibited similar suture retention strength and *ex vivo* sealing pressure to native tissues, indicating

their potential clinical utility, attributed to their enhanced suture-handling properties. Furthermore, the results showed the engineered scaffolds were highly biocompatible *in vitro*, and could promote the adhesion, proliferation and spreading of SMCs, urothelial cells as well as fibroblast cells. Taken together, our results suggest that GelMA/ELP fibrous scaffolds have the potential to be used for urologic reconstruction.

5. REFERENCES

[1] P. X. Ma, "Biomimetic materials for tissue engineering," *Advanced drug delivery reviews,* vol. 60, no. 2, pp. 184-198, 2008.

[2] M. Wang, P. Zhai, X. Chen, D. J. Schreyer, X. Sun, and F. Cui, "Bioengineered scaffolds for spinal cord repair," *Tissue Engineering Part B: Reviews,* vol. 17, no. 3, pp. 177-194, 2011.

[3] N. Lee, J. Robinson, and H. Lu, "Biomimetic strategies for engineering composite tissues," *Current opinion in biotechnology,* vol. 40, pp. 64-74, 2016.

[4] C. Chen *et al.*, "Bioinspired hydrogel electrospun fibers for spinal cord regeneration," *Advanced Functional Materials,* vol. 29, no. 4, p. 1806899, 2019.

[5] T. Mann and C. Lutwak-Mann, *Male reproductive function and semen: themes and trends in physiology, biochemistry and investigative andrology*. Springer Science & Business Media, 2012.

[6] N. Lumen, W. Oosterlinck, and P. Hoebeke, "Urethral reconstruction using buccal mucosa or penile skin grafts: systematic review and meta-analysis," *Urologia internationalis,* vol. 89, no. 4, pp. 387-394, 2012.

[7] B. N. Breyer *et al.*, "Multivariate analysis of risk factors for long-term urethroplasty outcome," *The Journal of urology,* vol. 183, no. 2, pp. 613-617, 2010.

[8] C. Heyns, J. Steenkamp, M. De Kock, and P. Whitaker, "Treatment of male urethral strictures: is repeated dilation or internal urethrotomy useful?," *The journal of Urology,* vol. 160, no. 2, pp. 356-358, 1998.

[9] R. R. Dmochowski, A. J. Wein, A. W. Partin, C. A. Peters, and L. R. Kavoussi, "Campbell-Walsh-Wein Urology Twelfth Edition Review E-Book," 2020.

[10] V. de Kemp, P. de Graaf, J. O. Fledderus, J. Ruud Bosch, and L. M. de Kort, "Tissue engineering for human urethral reconstruction: systematic review of recent literature," *PloS one,* vol. 10, no. 2, p. e0118653, 2015.

[11] M. Zamani, N. Shakhssalim, S. Ramakrishna, and M. Naji, "Electrospinning: application and prospects for urologic tissue engineering," *Frontiers in Bioengineering and Biotechnology,* vol. 8, p. 579925, 2020.

[12] Z. Rashidbenam *et al.*, "Overview of urethral reconstruction by tissue engineering: current strategies, clinical status and future direction," *Tissue engineering and regenerative medicine,* vol. 16, pp. 365-384, 2019.

[13] D. Wood, S. Allen, D. Andrich, T. Greenwell, and A. Mundy, "The morbidity of buccal mucosal graft harvest for urethroplasty and the effect of nonclosure of the graft harvest site on postoperative pain," *The Journal of urology,* vol. 172, no. 2, pp. 580-583, 2004.

[14] J. Kopeček, "Hydrogel biomaterials: a smart future?," *Biomaterials,* vol. 28, no. 34, pp. 5185-5192, 2007.

[15] X. Jia and K. L. Kiick, "Hybrid multicomponent hydrogels for tissue engineering," *Macromolecular bioscience,* vol. 9, no. 2, pp. 140-156, 2009.

[16] H. Samadian, H. Maleki, Z. Allahyari, and M. Jaymand, "Natural polymers-based light-induced hydrogels: Promising biomaterials for biomedical applications," *Coordination Chemistry Reviews,* vol. 420, p. 213432, 2020.

[17] X. Guan *et al.*, "Development of hydrogels for regenerative engineering," *Biotechnology journal,* vol. 12, no. 5, p. 1600394, 2017.

[18] S. J. Buwalda, K. W. Boere, P. J. Dijkstra, J. Feijen, T. Vermonden, and W. E. Hennink, "Hydrogels in a historical perspective: From simple networks to smart materials," *Journal of controlled release,* vol. 190, pp. 254-273, 2014.

[19] N. Annabi *et al.*, "25th anniversary article: Rational design and applications of hydrogels in regenerative medicine," *Advanced materials,* vol. 26, no. 1, pp. 85-124, 2014.

[20] K. Zhang *et al.*, "3D bioprinting of urethra with PCL/PLCL blend and dual autologous cells in fibrin hydrogel: An in vitro evaluation of biomimetic mechanical property and cell growth environment," *Acta biomaterialia,* vol. 50, pp. 154-164, 2017.

[21] W. Fu *et al.*, "Electrospun gelatin/PCL and collagen/PLCL scaffolds for vascular tissue engineering," *International journal of nanomedicine,* vol. 9, p. 2335, 2014.

[22] G. H. Altman *et al.*, "Silk-based biomaterials," *Biomaterials,* vol. 24, no. 3, pp. 401-416, 2003.

[23] K. Numata, B. Subramanian, H. A. Currie, and D. L. Kaplan, "Bioengineered silk protein-based gene delivery systems," *Biomaterials,* vol. 30, no. 29, pp. 5775-5784, 2009.

[24] U.-J. Kim, J. Park, H. J. Kim, M. Wada, and D. L. Kaplan, "Three-dimensional aqueous-derived biomaterial scaffolds from silk fibroin," *Biomaterials,* vol. 26, no. 15, pp. 2775-2785, 2005.

[25] Y. N. Zhang *et al.*, "A highly elastic and rapidly crosslinkable elastin-like polypeptide-based hydrogel for biomedical applications," *Advanced functional materials,* vol. 25, no. 30, pp. 4814-4826, 2015.

[26] B. P. Toole, "Hyaluronan: from extracellular glue to pericellular cue," *Nature Reviews Cancer,* vol. 4, no. 7, pp. 528-539, 2004.

[27] M. I. Bury *et al.*, "The promotion of functional urinary bladder regeneration using anti-inflammatory nanofibers," *Biomaterials,* vol. 35, no. 34, pp. 9311-9321, 2014.

[28] U. Özok, M. Eroğlu, A. İmamoğlu, H. Bakirtaş, N. Güvence, and A. Kİper, "Subureteral dextranomer/hyaluronic acid copolymer injection for vesicoureteral reflux in transplant candidates," *Journal of endourology,* vol. 19, no. 10, pp. 1185-1187, 2005.

[29] K. Y. Lee and D. J. Mooney, "Alginate: properties and biomedical applications," *Progress in polymer science,* vol. 37, no. 1, pp. 106-126, 2012.

[30] J. Kurowiak *et al.*, "Changes in the Mechanical Properties of Alginate-Gelatin Hydrogels with the Addition of Pygeum africanum with Potential Application in Urology," *International Journal of Molecular Sciences,* vol. 23, no. 18, p. 10324, 2022.

[31] M. Dash, F. Chiellini, R. M. Ottenbrite, and E. Chiellini, "Chitosan—A versatile semi-synthetic polymer in biomedical applications," *Progress in polymer science,* vol. 36, no. 8, pp. 981-1014, 2011.

[32] M. Hajiabbas *et al.*, "Chitosan-gelatin sheets as scaffolds for muscle tissue engineering," *Artificial Cells, Nanomedicine, and Biotechnology,* vol. 43, no. 2, pp. 124-132, 2015.

[33] S. Wu, Y. Liu, S. Bharadwaj, A. Atala, and Y. Zhang, "Human urine-derived stem cells seeded in a modified 3D porous small intestinal submucosa scaffold for urethral tissue engineering," *Biomaterials,* vol. 32, no. 5, pp. 1317-1326, 2011.

[34] E. Palminteri, E. Berdondini, F. Colombo, and E. Austoni, "Small intestinal submucosa (SIS) graft urethroplasty: short-term results," *European urology,* vol. 51, no. 6, pp. 1695-1701, 2007.

[35] R. Fiala, A. Vidlar, R. Vrtal, K. Belej, and V. Student, "Porcine small intestinal submucosa graft for repair of anterior urethral strictures," *European urology,* vol. 51, no. 6, pp. 1702-1708, 2007.

[36] M. Raber *et al.*, "Dorsal onlay graft urethroplasty using penile skin or buccal mucosa for repair of bulbar urethral stricture: results of a prospective single center study," *European urology,* vol. 48, no. 6, pp. 1013-1017, 2005.

[37] W. Chen, J. Kumari, H. Yuan, F. Yang, and P. H. Kouwer, "Toward Tissue-Like Material Properties: Inducing In Situ Adaptive Behavior in Fibrous Hydrogels," *Advanced Materials,* vol. 34, no. 37, p. 2202057, 2022.

[38] M. A. Pattison, S. Wurster, T. J. Webster, and K. M. Haberstroh, "Three-dimensional, nano-structured PLGA scaffolds for bladder tissue replacement applications," *Biomaterials,* vol. 26, no. 15, pp. 2491-2500, 2005.

[39] A. Kanematsu, S. Yamamoto, T. Noguchi, M. Ozeki, Y. Tabata, and O. Ogawa, "Bladder regeneration by bladder acellular matrix combined with sustained release of exogenous growth factor," *The Journal of urology,* vol. 170, no. 4 Part 2, pp. 1633-1638, 2003.

[40] I. Stanasel, M. Mirzazadeh, and J. J. Smith, "Bladder tissue engineering," *Urologic Clinics,* vol. 37, no. 4, pp. 593-599, 2010.

[41] L. R. Versteegden *et al.*, "Tubular collagen scaffolds with radial elasticity for hollow organ regeneration," *Acta biomaterialia,* vol. 52, pp. 1-8, 2017.

[42] Q. Pi *et al.*, "Digitally tunable microfluidic bioprinting of multilayered cannular tissues," *Advanced Materials,* vol. 30, no. 43, p. 1706913, 2018.

[43] P. Joshi, C. Kaya, and S. Kulkarni, "Approach to bulbar urethral strictures: Which technique and when?," *Turkish journal of urology,* vol. 42, no. 2, p. 53, 2016.

[44] T. Ishii, C. K. Ho, H. Nahas, B. Y. Yiu, A. J. Chee, and A. C. Yu, "Deformable phantoms of the prostatic urinary tract for urodynamic investigations," *Medical Physics,* vol. 46, no. 7, pp. 3034-3043, 2019.

[45] S. Pisani, R. Dorati, B. Conti, T. Modena, G. Bruni, and I. Genta, "Design of copolymer PLA-PCL electrospun matrix for biomedical applications," *Reactive and Functional Polymers,* vol. 124, pp. 77-89, 2018.

[46] A. Raya-Rivera, D. R. Esquiliano, J. J. Yoo, E. Lopez-Bayghen, S. Soker, and A. Atala, "Tissue-engineered autologous urethras for patients who need reconstruction: an observational study," *The lancet,* vol. 377, no. 9772, pp. 1175-1182, 2011.

[47] D. H. Reneker and A. L. Yarin, "Electrospinning jets and polymer nanofibers," *Polymer,* vol. 49, no. 10, pp. 2387-2425, 2008.

[48] Z.-M. Huang, Y.-Z. Zhang, M. Kotaki, and S. Ramakrishna, "A review on polymer nanofibers by electrospinning and their applications in nanocomposites," *Composites science and technology,* vol. 63, no. 15, pp. 2223-2253, 2003.

[49] S. Agarwal, J. H. Wendorff, and A. Greiner, "Use of electrospinning technique for biomedical applications," *Polymer,* vol. 49, no. 26, pp. 5603-5621, 2008.

[50] T. J. Sill and H. A. Von Recum, "Electrospinning: applications in drug delivery and tissue engineering," *Biomaterials,* vol. 29, no. 13, pp. 1989-2006, 2008.

[51] C. Feng, C. Liu, S. Liu, Z. Wang, K. Yu, and X. Zeng, "Electrospun nanofibers with core–shell structure for treatment of bladder regeneration," *Tissue Engineering Part A,* vol. 25, no. 17-18, pp. 1289-1299, 2019.

[52] S. Sivaraman *et al.*, "Evaluation of poly (Carbonate-Urethane) urea (PCUU) scaffolds for urinary bladder tissue engineering," *Annals of biomedical engineering,* vol. 47, pp. 891-901, 2019.

[53] M. Horst, V. Milleret, S. Noetzli, R. Gobet, T. Sulser, and D. Eberli, "Polyesterurethane and acellular matrix based hybrid biomaterial for bladder engineering," *Journal of Biomedical Materials Research Part B: Applied Biomaterials,* vol. 105, no. 3, pp. 658-667, 2017.

[54] M. Horst, S. Madduri, V. Milleret, T. Sulser, R. Gobet, and D. Eberli, "A bilayered hybrid microfibrous PLGA–acellular matrix scaffold for hollow organ tissue engineering," *Biomaterials,* vol. 34, no. 5, pp. 1537-1545, 2013.

[55] J. W. Huang *et al.*, "Tissue performance of bladder following stretched electrospun silk fibroin matrix and bladder acellular matrix implantation in a rabbit model," *Journal of biomedical materials research Part A,* vol. 104, no. 1, pp. 9-16, 2016.

[56] X. Lv *et al.*, "Electrospun poly (l-lactide)/poly (ethylene glycol) scaffolds seeded with human amniotic mesenchymal stem cells for urethral epithelium repair," *International Journal of Molecular Sciences,* vol. 17, no. 8, p. 1262, 2016.

[57] F. Sharifiaghdas *et al.*, "Comparing supportive properties of poly lactic-co-glycolic acid (PLGA), PLGA/collagen and human amniotic membrane for human urothelial and smooth muscle cells engineering," *Urology Journal,* vol. 11, no. 3, pp. 1620-1628, 2014.

[58] N. Shakhssalim, J. Rasouli, R. Moghadasali, F. S. Aghdas, M. Naji, and M. Soleimani, "Bladder smooth muscle cells interaction and proliferation on PCL/PLLA electrospun nanofibrous scaffold," *The International Journal of Artificial Organs,* vol. 36, no. 2, pp. 113-120, 2013.

[59] K. Xu, Y. Han, Y. Huang, P. Wei, J. Yin, and J. Jiang, "The application of 3D bioprinting in urological diseases," *Materials Today Bio,* p. 100388, 2022.

[60] S. Vijayavenkataraman, W.-C. Yan, W. F. Lu, C.-H. Wang, and J. Y. H. Fuh, "3D bioprinting of tissues and organs for regenerative medicine," *Advanced drug delivery reviews,* vol. 132, pp. 296-332, 2018.

[61] R. Sartoneva *et al.*, "Characterizing and optimizing poly-L-lactide-co-ε-caprolactone membranes for urothelial tissue engineering," *Journal of The Royal Society Interface,* vol. 9, no. 77, pp. 3444-3454, 2012.

[62] M. Volpi, A. Paradiso, M. Costantini, and W. Święszkowski, "Hydrogel-based fiber biofabrication techniques for skeletal muscle tissue engineering," *ACS Biomaterials Science & Engineering,* vol. 8, no. 2, pp. 379-405, 2022.

[63] J. W. Nichol, S. T. Koshy, H. Bae, C. M. Hwang, S. Yamanlar, and A. Khademhosseini, "Cell-laden microengineered gelatin methacrylate hydrogels," *Biomaterials,* vol. 31, no. 21, pp. 5536-5544, 2010.

[64] M. Lin, S. Rose-John, J. Grötzinger, U. Conrad, and J. Scheller, "Functional expression of a biologically active fragment of soluble gp130 as an ELP-fusion protein in transgenic plants: purification via inverse transition cycling," *Biochemical Journal,* vol. 398, no. 3, pp. 577-583, 2006.

[65] L. L. Palmese, R. K. Thapa, M. O. Sullivan, and K. L. Kiick, "Hybrid hydrogels for biomedical applications," *Current opinion in chemical engineering,* vol. 24, pp. 143-157, 2019.

[66] E. Shirzaei Sani *et al.*, "Engineering adhesive and antimicrobial hyaluronic acid/elastin-like polypeptide hybrid hydrogels for tissue engineering applications," *ACS biomaterials science & engineering,* vol. 4, no. 7, pp. 2528-2540, 2018.

[67] K. Yue, G. Trujillo-de Santiago, M. M. Alvarez, A. Tamayol, N. Annabi, and A. Khademhosseini, "Synthesis, properties, and biomedical applications of gelatin methacryloyl (GelMA) hydrogels," *Biomaterials,* vol. 73, pp. 254-271, 2015.

[68] S. R. MacEwan and A. Chilkoti, "Elastin-like polypeptides: biomedical applications of tunable biopolymers," *Peptide Science: Original Research on Biomolecules,* vol. 94, no. 1, pp. 60-77, 2010.

[69] W. F. Daamen, J. Veerkamp, J. Van Hest, and T. Van Kuppevelt, "Elastin as a biomaterial for tissue engineering," *Biomaterials,* vol. 28, no. 30, pp. 4378-4398, 2007.

[70] D. L. Nettles, A. Chilkoti, and L. A. Setton, "Applications of elastin-like polypeptides in tissue engineering," *Advanced drug delivery reviews,* vol. 62, no. 15, pp. 1479-1485, 2010.

[71] S. S. Mahdavi, M. J. Abdekhodaie, S. Mashayekhan, A. Baradaran-Rafii, and K. Kim, "Development and in vitro evaluation of photocurable GelMA/PEGDA hybrid hydrogel for corneal stromal cells delivery," *Materials Today Communications,* vol. 27, p. 102459, 2021.

[72] I. Noshadi *et al.*, "In vitro and in vivo analysis of visible light crosslinkable gelatin methacryloyl (GelMA) hydrogels," *Biomaterials science,* vol. 5, no. 10, pp. 2093-2105, 2017.

[73] J. A. Burdick and G. D. Prestwich, "Hyaluronic acid hydrogels for biomedical applications," *Advanced materials,* vol. 23, no. 12, pp. H41-H56, 2011.

[74] Y. Li, J. Wang, Y. Wang, and W. Cui, "Advanced electrospun hydrogel fibers for wound healing," *Composites Part B: Engineering,* vol. 223, p. 109101, 2021.

[75] G. Unal *et al.*, "Engineering elastic sealants based on gelatin and elastin-like polypeptides for endovascular anastomosis," *Bioengineering & translational medicine,* vol. 6, no. 3, p. e10240, 2021.

[76] J. Yang, Y. S. Zhang, K. Yue, and A. Khademhosseini, "Cell-laden hydrogels for osteochondral and cartilage tissue engineering," *Acta biomaterialia,* vol. 57, pp. 1-25, 2017.

[77] L. Martinez-Vidal *et al.*, "Causal contributors to tissue stiffness and clinical relevance in urology," *Communications Biology,* vol. 4, no. 1, p. 1011, 2021.

[78] A. M. Coenen, K. V. Bernaerts, J. A. Harings, S. Jockenhoevel, and S. Ghazanfari, "Elastic materials for tissue engineering applications: Natural, synthetic, and hybrid polymers," *Acta biomaterialia,* vol. 79, pp. 60-82, 2018.

[79] J. Booth, L. Connelly, S. Dickson, F. Duncan, and M. Lawrence, "The effectiveness of transcutaneous tibial nerve stimulation (TTNS) for adults with overactive bladder syndrome: a systematic review," *Neurourology and urodynamics,* vol. 37, no. 2, pp. 528-541, 2018.

[80] Q. T. Nguyen, Y. Hwang, A. C. Chen, S. Varghese, and R. L. Sah, "Cartilage-like mechanical properties of poly (ethylene glycol)-diacrylate hydrogels," *Biomaterials,* vol. 33, no. 28, pp. 6682-6690, 2012.

[81] X. Meng, X. Wang, Y. Jiang, B. Zhang, K. Li, and Q. Li, "Suture retention strength of P (LLA-CL) tissue-engineered vascular grafts," *RSC advances,* vol. 9, no. 37, pp. 21258-21264, 2019.

[82] A. S. Hoffman, "Hydrogels for biomedical applications," *Advanced drug delivery reviews,* vol. 64, pp. 18-23, 2012.

[83] C. B. Highley, C. B. Rodell, and J. A. Burdick, "Direct 3D printing of shear-thinning hydrogels into self-healing hydrogels," *Advanced Materials,* vol. 27, no. 34, pp. 5075-5079, 2015.

[84] J. L. Drury and D. J. Mooney, "Hydrogels for tissue engineering: scaffold design variables and applications," *Biomaterials,* vol. 24, no. 24, pp. 4337-4351, 2003.

[85] A. Yeboah, R. I. Cohen, C. Rabolli, M. L. Yarmush, and F. Berthiaume, "Elastin-like polypeptides: A strategic fusion partner for biologics," *Biotechnology and bioengineering,* vol. 113, no. 8, pp. 1617-1627, 2016.

[86] B. V. Slaughter, S. S. Khurshid, O. Z. Fisher, A. Khademhosseini, and N. A. Peppas, "Hydrogels in regenerative medicine," *Advanced materials,* vol. 21, no. 32-33, pp. 3307-3329, 2009.

[87] H. Kamata, X. Li, U. i. Chung, and T. Sakai, "Design of hydrogels for biomedical applications," *Advanced healthcare materials,* vol. 4, no. 16, pp. 2360-2374, 2015.

[88] T. N. Vo, F. K. Kasper, and A. G. Mikos, "Strategies for controlled delivery of growth factors and cells for bone regeneration," *Advanced drug delivery reviews,* vol. 64, no. 12, pp. 1292-1309, 2012.

[89] H. Birkedal-Hansen, "Role of cytokines and inflammatory mediators in tissue destruction," *Journal of periodontal research,* vol. 28, no. 7, pp. 500-510, 1993.

[90] R. R. Resende *et al.*, "Scale/topography of substrates surface resembling extracellular matrix for tissue engineering," *Journal of Biomedical Nanotechnology,* vol. 10, no. 7, pp. 1157-1193, 2014.

[91] R. G. Flemming, C. J. Murphy, G. A. Abrams, S. L. Goodman, and P. F. Nealey, "Effects of synthetic micro-and nano-structured surfaces on cell behavior," *Biomaterials,* vol. 20, no. 6, pp. 573-588, 1999.

[92] V. Karageorgiou and D. Kaplan, "Porosity of 3D biomaterial scaffolds and osteogenesis," *Biomaterials,* vol. 26, no. 27, pp. 5474-5491, 2005.

[93] S. J. Hollister, "Porous scaffold design for tissue engineering," *Nature materials,* vol. 4, no. 7, pp. 518-524, 2005.

[94] A. J. Engler, S. Sen, H. L. Sweeney, and D. E. Discher, "Matrix elasticity directs stem cell lineage specification," *Cell,* vol. 126, no. 4, pp. 677-689, 2006.

[95] H. Gray, S. Standring, H. Ellis, and B. Berkovitz, "Gray's anatomy: the anatomical basis of clinical practice," *(No Title),* 2008.

[96] R. M. Hicks, "The mammalian urinary bladderan accommodating organ," *Biological Reviews,* vol. 50, no. 2, pp. 215-246, 1975.